JTTEE5 15:400-412
DOI: 10.1361/105996306X124400
1059-9630/$19.00 © ASM International

Peer Reviewed

Investigation and Characterization of Cr_3C_2-Based Wear-Resistant Coatings Applied by the Cold Spray Process

Douglas E. Wolfe, Timothy J. Eden, John K. Potter, and Adam P. Jaroh

(Submitted August 18, 2005; in revised form January 9, 2006)

The purpose of this study was to explore the potential of the cold spray (CS) process in applying Cr_3C_2-25wt.%NiCr and Cr_3C_2-25wt.%Ni coatings on 4140 alloy for wear-resistant applications. This article discusses the improvements in Cr_3C_2-based coating properties and microstructure through changes in nozzle design, powder characteristics, standoff distance, powder feed rate, and traverse speed that resulted in an improved average Vickers hardness number comparable to some thermal spray processes. Cold spray process optimization of the Cr_3C_2-based coatings resulted in increased hardness and improved wear characteristics with lower friction coefficients. The improvement in hardness is directly associated with higher particle velocities and increased densities of the Cr_3C_2-based coatings deposited on 4140 alloy at ambient temperature. Selective coatings were evaluated using x-ray diffraction for phase analysis, optical microscopy (OM), and scanning electron microscopy (SEM) for microstructural evaluation, and ball-on-disk tribology experiments for friction coefficient and wear determination. The presented results strongly suggest that cold spray is a versatile coating technique capable of tailoring the hardness of Cr_3C_2-based wear-resistant coatings on temperature sensitive substrates.

Keywords cold gas dynamic spraying, composite materials, influence of spray parameters, wear

1. Introduction

The cold spray process technology was originally developed at the Institute of Theoretical and Applied Mechanics of the Siberian Division of the Russian Academy of Science in Novosibirsk in the mid-1980s and later patented in the United States in 1994 as part of U.S. interest in Russian technology (Ref 1). Since then, the cold spray process has been referred to as cold gas dynamic-spray (CGDS) (Ref 2), high-velocity particle consolidation (HVPC) (Ref 3), cold gas spray (CGS) (Ref 4, 5), and kinetic spray (KS) (Ref 6, 7). Anatoli Papyrin, the inventor of the cold spray process, along with other researchers, has shown that the cold spray technology can be used to apply a wide variety of metallic, dielectric (ceramic), metallic alloys, and mixed combinations on a variety of substrate material (Ref 3, 8-11). In general, thermal spray coating processes are classified into two classifications: (a) temperature-based, where feedstock material is rendered molten (or partially molten) through its introduction into intense heat such as an arc, plasma, or flame prior to impingement onto a substrate (i.e., D-gun, plasma spray, and arc spray processes), and (b) velocity-based processes employing high particle velocities and accelerations, lower particle feedstock material temperatures, and shorter transient times (i.e., cold spray, high-velocity air fuel [HVAF]), and high-velocity oxyfuel (HVOF). In HVAF and HVOF, partial melting of powders may still occur depending on the process parameters. Figure 1 illustrates typical particle velocities and gas temperatures for the primary thermal spray coating processes. As shown in Fig. 1, gas temperatures in the cold spray process are the lowest of the thermal spray coating processes, and the feedstock particle velocities are some of the highest. The major difference that separates the cold spray process from the conventional thermal spray coating processes is that during the cold spray process the feedstock material does not become molten or partially molten and deposits in the solid state due to plastic deformation (Ref 12-14).

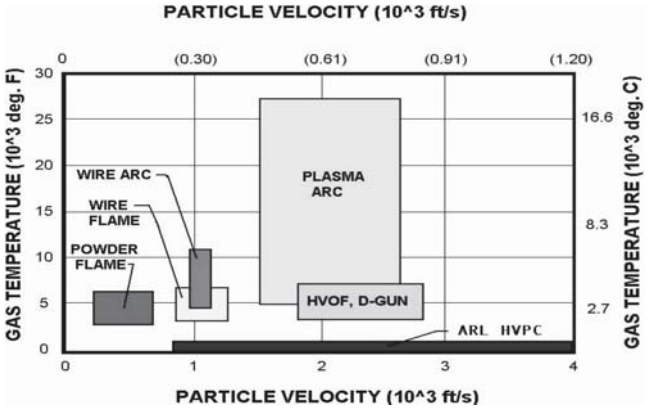

Fig. 1 Temperature and pressure regimes of the various thermal spray processes including wire arc, wire flame, powder flame, plasma arc, HVOF, D-gun, and cold spray

Figure 2 illustrates the cold spray process, in which compressed gas (typically, air, nitrogen, or helium) at pressures from 1 to 3 MPa is expanded through a converging-diverging (de Laval) nozzle where it leaves the nozzle at supersonic speeds (180

Douglas E. Wolfe, Timothy J. Eden, John K. Potter, and **Adam P. Jaroh,** Applied Research Laboratory, The Pennsylvania State University, University Park, PA 16802. Contact e-mail: dew125@psu.edu.

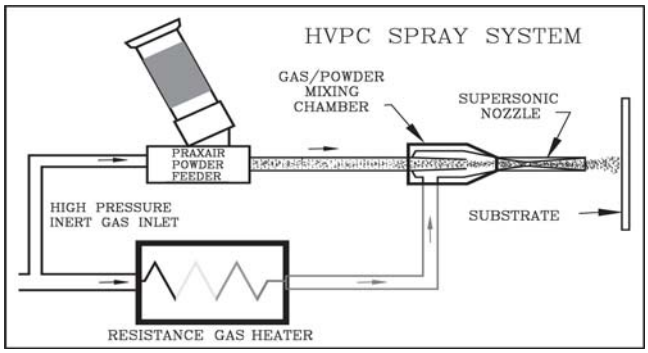

Fig. 2 Cold spray process

to 1200 m/s). Typically, the powder feedstock is introduced into the gas flow slightly upstream of the converging portion of the nozzle. The expanding gas rapidly accelerates the feedstock powder to very high velocities. Velocities range from 180 to 1200 m/s depending on nozzle design, powder characteristics (i.e., density, type, particle size distribution) gas type (N_2, He, air), temperature, and material (Ref 3, 15). A gas heater is generally used to increase the gas temperature prior to entering the de Laval nozzle and results in increased gas velocity and particle temperature. In general, heating the particle increases the ductility of the particle and results in increased deposition efficiencies allowing coatings to build up quicker. Within the diverging portion of the de Laval nozzle, gas rapidly expands causing the gas temperature to drop. As particles are accelerated, they begin to cool, but since the residence time in the nozzle is short, the particle temperature decrease is relatively small. As the particles impact and bond (plastically deform) to a substrate positioned up to 25.4 mm (standoff distance) from the exit plane of the nozzle, the coating thickness increases. This standoff distance can be adjusted to change the width of the coating, deposition rate, and sticking efficiency.

Some limitations of conventional thermal spray processes are addressed by the cold spray process (Ref 3). Due to the high deposition temperature of conventional thermal spray processes, limitations exist with the substrate materials that can be coated. Coating materials that undergo phase transformations, recrystallization, excessive oxidation, and evaporation may be difficult or impossible to apply using conventional thermal spray methods. This is especially true for reactive materials such as titanium. Deformation or increased residual stresses induced by the thermal coefficient of expansion mismatch that develop as the coating and substrate cool down after deposition (or after each spray pass) are common in thermal spray processes. Even if the coating remains attached to the substrate, high residual tensile stresses may cause unacceptable distortions that significantly weaken the bond strength, accelerate fatigue failures, and introduce microcracking, reducing the performance of the coating. Cold spray addresses some of these issues associated with conventional thermal spray techniques. The lower deposition temperatures reduce the effects associated with recrystallization in both the substrate and coating. Oxidation of metallic species is greatly reduced, which generally increases coating performance in corrosion environments. Cold spray technology can be applied to a wider variety of substrates, and residual stresses are generally compressive in nature, due to the physics of the impinging particles. Thick coatings can readily be built up, making cold spray technology a viable candidate for rapid prototyping. Noise levels are significantly lower, and there are no dangerous metal vapor fumes (however, depending on the size of the powders, necessary precautions should always be taken to prevent inhalation) (Ref 3, 8, 9).

Table 1 Typical cold spray processing parameters

Gas type	T_g, °C	P_g, MPa	Traverse rate, mm/s	Stand-off distance, mm	Powder flow, g/min	Coating thickness, µm
N_2	500	2.41	19-54	12.5-25.4	5.67-7.94	>1000

The presented efforts to investigate the process and alternative coating material systems were explored to expand the future capabilities of the cold spray process. It should be noted that the authors are not suggesting that cold spray will replace HVOF or other thermal spray processes for applying wear-resistant coatings, but rather are investigating the tailorability of coating properties such as wear, corrosion resistance, and average Vickers hardness numbers. The authors believe that cold spray processes will eventually excel with niche coating applications, such as corrosion-resistant coatings, sealants, and repair technology, in addition to microelectronic and biomedical applications.

2. Experimental

Using the unique, flexible cold spray facility at the Applied Research Laboratory, The Pennsylvania State University (ARL-PSU), various Cr_3C_2-based coatings were applied on 25.4 × 25.4 × 6.35 mm 4140 alloy steel. The feedstock powder was baked out in an oven at 150 °F to remove moisture and improve powder flowability. The powder was then weighed and placed in the Praxair model number 1264 HPHV powder feeder (Praxair Surface Technologies, Concord, NH). Prior to spraying the coatings, the 4140 substrates were grit blasted (TRINCO Dry Blast, Trinity Tool Co., Fraser, MI) using 16 to 20 grit aluminum oxide powder (TRINCO, Trinity Tool Co., Fraser, MI) to remove surface oxides and create a minimum surface finish of approximately R_a equal to 200 µin. (5.08 µm). To increase the mechanical bonding between the cold sprayed coating and the substrate, a minimum surface roughness is desired but depends on substrate hardness. The 4140 alloy was then ultrasonically cleaned in ethyl alcohol to remove dirt and oil. The samples were then measured and weighed before being positioned in the tooling assembly with the desired standoff distance. A final ethyl alcohol rinse followed with compressed air drying was performed just prior to coating deposition to minimize contamination.

Based on the powder formulation, adjustments were made to the powder flow, gas temperature, nitrogen gas pressure, standoff distance, and traverse speed in an effort to optimize the coating density and thus average Vickers hardness number. Typical cold spray processing parameters for select Cr_3C_2-based coatings are listed in Tables 1 and 2. Details regarding the powder characteristics (i.e., particle size, morphology, powder size distribution, and density) are discussed in more detail in the next section.

Table 2 Sample series number and powder type description

Sample No.	Powder type and supplier
C1	100% nickel (Novamet)
C2	PSU blend 1: Cr_3C_2 (Cerac)-25wt.%Ni (Novamet)
C3	PSU blend 2: Cr_3C_2 (Cerac)-25wt.%Ni (Novamet)
C4	PSU blend 9: Cr_3C_2 (AEE)-18wt.%Ni (Novamet)
C5	PSU blend 3: Cr_3C_2 (AEE)-15wt.%Ni (Novamet)
C6	TAFA 1375V: Cr_3C_2-25wt.%NiCr
C7	Praxair 1375VM: Cr_3C_2-25wt.%NiCr

Due to the hardness of the Cr_3C_2 powders, the stainless steel nozzle typically used in aluminum (Al) cold spray applications could not be used. Therefore, a proprietary tungsten carbide cobalt (WC-Co) nozzle was designed and fabricated to improve the coating process. The particle velocity calculations using the Sandia code (Ref 16) suggested a 25% increase in particle velocity based on the nozzle design. The higher particle velocity resulting from the improved nozzle design resulted in increased coating density and thus increased average Vickers hardness number of ~20%, as is discussed later.

The nozzle and gas heater of the ARL-PSU cold spray unit are mounted on a six-axis robot enclosed in an acoustic room to minimize noise levels. In addition, the robot uses a multiaxis turntable (capable of holding up to 100 kg) for coating complex geometries. The gas and overspray that flow through the nozzle were collected inside the acoustic room and carried to a dust collector trapping all particulates down to the submicron level. To collect and recycle powders, a cyclone separator could be positioned in line. Nitrogen gas at pressures up to 1.6 MPa was supplied by vaporizing liquid nitrogen from a large tank. When higher nitrogen pressures were required, a booster pump was used to increase the pressure up to 3.1 MPa.

In this investigation, the coatings were applied to a minimum thickness of 1000 μm. After the desired coating thickness was applied, the cold spray unit was turned off, the samples were allowed to cool, and then measurements and weights were taken. Prior to the tribology testing, the cold spray coatings were machined to approximately 890 μm in thickness with a surface finish of R_a = 24 to 70 μin. (0.61 to 1.78 μm). The surface finish of the coatings varied for the select coating due to the type of powder and coating microstructure (i.e., porosity). Using a portable Federal Pocket Surf III surface roughness instrument (Mahr Federal Products Company, Providence, RI), the surface finish of each sample was measured and recorded. One sample from each lot was used for microstructural investigation. Using a LECO diamond wafering saw (LECO Corp., St. Joseph, MO), sections of the samples were made and mounted in epoxy for coating cross-sectional analysis. Select sample cross sections were then examined using optical microscopy (OM) and scanning electron microscopy (SEM). A variety of characterization techniques were used to determine the average Vickers hardness number, particle size distribution, particle density, select bond strength, and tribological properties (i.e., wear rate and friction coefficients). The Vickers hardness measurements were made using a LECO model M-400-G1 hardness tester (LECO Corp.) with a 300 g load on the polished cross section of the coatings. A minimum of 10 to 15 indentations were made for each specimen with the average value being reported. Normal Bragg-Brantano ($\theta/2\theta$) x-ray diffraction (XRD) continuous scans were performed using Cu Kα1 radiation = 0.154056 nm, Cu Kα2 = 0.154056 nm wavelength, over the range of 2θ = 30 to 80° at 2 s per step with a step size of 0.030° to determine crystallographic orientation and phase analysis. Finally, preliminary investigation of combining the cold spray process with laser processing in an effort to further improve the average Vickers hardness number and thus wear-resistant properties of the coating were investigated. The results strongly suggest that a hybrid technique could substantially improve the quality of cold spray wear-resistant coatings. Selective results are presented.

3. Results and Discussion

In general, increased wear resistance occurs with increasing hardness values. In the cold spray process, as the particles impinge on the substrate material, coating buildup relies on plastic deformation. Hard, ceramic particles such as chromium carbide, titanium carbide, and tungsten carbide will not plastically deform to allow coating to build up. Therefore, a softer binder material is added for coating deposition. The most common Cr_3C_2-based coating formulation is Cr_3C_2-25wt.%NiCr. Various aspects of the CS process were examined in this investigation including substrate surface finish, processing parameters (Table 1), and powder characteristics, in an effort to better understand the role of various factors on the average Vickers hardness value of the Cr_3C_2-based coatings and wear-resistance performance. The primary factors that affect particle velocity (and thus coating density and hardness) are: increased gas temperature, increased pressure, type of gas (use helium versus nitrogen, but more expensive), powder characteristics (particle size, morphology, size distribution, and density), nozzle design, standoff distance, powder feed rate, traverse speed, and type and volume of wear-resistant particles (i.e., Cr_3C_2 versus WC).

3.1 Average Vickers Hardness Number

Preliminary cold spray trials resulted in average Vickers hardness numbers (HV) for Cr_3C_2-25wt.%NiCr in the low to high 300 $HV_{0.300}$ range. The lower-than-expected hardness values were attributed to the increase in coating porosity (i.e., lower coating density). Since hardness is often correlated with wear resistance, CS process refinement and powder characteristics (including composition) were performed in an effort to increase the coating density, and thus HV. Processing parameters such as standoff distance, traverse rate, powder feed rate, and nozzle design were investigated for various Cr_3C_2-based powders C3, C4, C5, and C6 and are shown in Fig. 3(a). The average Vickers Hardness Number for the uncoated 4140 alloy and pure nickel powder (used in the blends) are included for reference (Fig. 3a).

Trends were observed as a function of the various processing parameters. In general, the average Vickers hardness number increased with decreasing standoff distance, decreased traverse rate, and improved nozzle design. Using the newly designed WC-Co nozzle, a 17% increase in the HV was obtained and was attributed to an increase in particle velocity resulting in increased density. Using the Sandia code, the Cr_3C_2-25NiCr particle velocity was calculated as a function of the nozzle inlet pressure (psi) for three of ARL-PSU nozzle designs. As shown

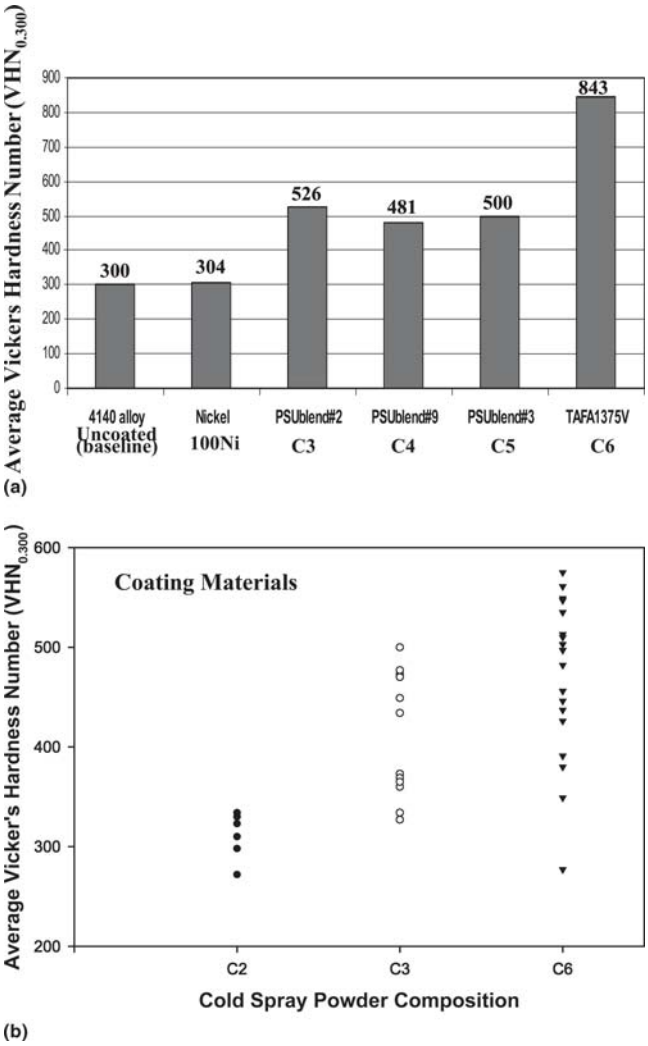

Fig. 3 (a) Average Vickers hardness number ($HV_{0.300}$) for uncoated and coated nickel, agglomerated and sintered (C6: TAFA 1375, Cr_3C_2-NiCr), and blended (Cr_3C_2-Ni: C3, C4, and C5) coatings applied by cold spray process. (b) Tailored average Vickers hardness number ($HV_{0.300}$) for cold spray coatings C2 (272 to 334 $HV_{0.300}$), C3 (327 to 504 $HV_{0.300}$), and C6 (277 to 575 $HV_{0.300}$) deposited under various conditions showing a wide range of tailored hardness values

in Fig. 4, almost a 25% (100 m/s increase) in the particle velocity was obtained with the newly designed nozzle. In addition, a 37% increase in the average Vickers hardness number was obtained by decreasing the nozzle traverse speed from 54 to 19 mm/s. Finally, a 29% improvement in HV was observed by decreasing the standoff distance from 25.4 to 19 mm. The optimal processing conditions for TAFA 1375V powder (TAFA Inc., Concord, NH) using the 3 mm throat/153 mm length WC-Co nozzle were determined to be: gas temperature: 500 °C, gas pressure: 2.41 MPa, standoff distance: 19 mm, traverse speed: 19 mm/s, and powder feed rate: 5.67 to 7.94 g/min. A 57% improvement in Vickers hardness number (549 $HV_{0.500}$) for Cr_3C_2-25wt.%NiCr coatings deposited on 4140 alloy is realized through these optimizations.

In a parallel effort, pure nickel (soft matrix) and Cr_3C_2 (wear-resistant) powders were mixed "in-house" (PSU blend: Cr_3C_2-

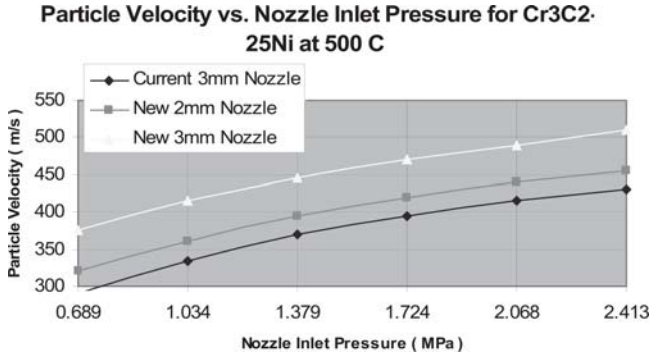

Fig. 4 Particle velocity predicted by a one-dimensional gas dynamic model, which predicts a higher velocity for a longer nozzle

25wt.%Ni) to further improve CS coating performance. Two different particle size distributions [PSU blend No. 1 (C2) and PSU blend No. 2 (C3)] of Cr_3C_2 powder were mixed in an attempt to increase the volume fraction of hard particles (Cr_3C_2) incorporated within the cold spray coating. The hardness of the PSU blend coating was increased by 29% up to 373 $HV_{0.500}$. Although the coating density was significantly improved over the prealloyed TAFA 1375V powder, the average Vickers hardness number remained low due to insufficient hard particle incorporation. Comparison of the PSU blend and TAFA 1375V coating cross section shows a larger volume percent of Cr_3C_2 in the TAFA 1375V, as discussed in Section 3.4.

Through investigation of the various processing parameters, it was determined that the HV could be tailored to a particular number. Figure 3(b) shows selective average Vickers hardness numbers for compositions C2, C3, and C6 for samples deposited under a variety of cold spray conditions (not listed). As seen in Fig. 3(b), the HV can be controlled over a wide range of hardness values, which allows tailorability of the coating hardness values for specific applications in which the mating surface may have to be matched in hardness value. Under the parameters studied, the $HV_{0.300}$ values ranged from 272 to 334 $HV_{0.300}$, 327 to 500 $HV_{0.300}$, and 277 to 575 $HV_{0.300}$ for C2, C3, and C6, respectively. Further refinements were also made in which the $HV_{0.300}$ was further increased for some of the various powders investigated (i.e., 843 $HV_{0.300}$ for TAFA 1375V).

Once the optimal Cr_3C_2 powder characteristics are identified, it is anticipated that MoS_2, a solid lubricant, will be incorporated into both candidate wear-resistant coatings to reduce the friction coefficient. Reducing the friction coefficient of the coating should result in improved wear-resistance properties. In addition to adding solid lubricants, bead peening and laser glazing of the coatings are being explored to densify the coating to improve the coating hardness and further improve wear-resistance properties.

3.2 Powder Characteristics

Various powder formulations were sprayed in an effort to tailor the average Vickers hardness number of cold spray coatings and determine the maximum value for several blended formulations. Table 3 briefly describes the chemical composition and production method of the various powders used in this in-

Table 3 Chemical composition and production method of cold spray powder feed stock

Powder	Powder supplier	Primary composition	Production method	Cr	C	Ni
Ni (C1)	Novamet	100% Ni	Thermal decomposition	0 ppm	430 ppm	bal
Cr_3C_2 (−325 mesh)	Cerac	100% Cr_3C_2	Crushed grinding and sintered	86.43 wt.%	13.16 wt.%	NA
Cr_3C_2 (−200/+325 mesh)	Cerac	100% Cr_3C_2	Crushed grinding and sintered	86.53 wt.%	12.87 wt.%	NA
Cr_3C_2	AEE	100% Cr_3C_2	Sintered	86.45 wt.%	13.28 wt.%	NA
TAFA 1375V (C6)	TAFA	Cr_3C_2-25wt.%NiCr	Agglomerated and sintered	bal	ND	ND
Praxair 1375V	Praxair	Cr_3C_2-25wt.%NiCr	Agglomerated and sintered	bal	10 wt.%	19 wt.%
PSU blend 1 (C2)	Cerac/Novamet	Cr_3C_2-25wt.%Ni	Blended	bal	9.96 wt.%	25 wt.%
PSU blend 2 (C3)	Cerac/Novamet	Cr_3C_2-25wt.%Ni	Blended	bal	9.96 wt.%	25 wt.%
PSU blend 3 (C5)	AEE/Novamet	Cr_3C_2-15wt.%Ni	Blended	bal	11.29 wt.%	15 wt.%
PSU blend 9 (C4)	AEE/Novamet	Cr_3C_2-18wt.%Ni	Blended	bal	10.89 wt.%	18 wt.%

Table 4 Select powder characteristics

Powder	Supplier	Composition	$D(v, 0.1)$, μm	$D(v, 0.5)$, μm	$D(v, 0.9)$, μm	PSD	ρ, g/cm^3	$\rho_{theoretical}$, %
Ni	Novamet	100% Nickel	7.46	15.72	37.15	Broad	8.4886	95.6
Cr_3C_2	AEE	100% Cr_3C_2	45.13	65.35	93.15	Narrow	5.5496	82.0
TAFA 1375V	TAFA	Cr_3C_2-25wt.%NiCr	18.83	35.36	59.08	Broad	7.2947	>99.0
Praxair 1375V	Praxair	Cr_3C_2-25wt.%NiCr	21.36	34.22	52.64	Narrow	6.6531	92.3
Praxair 1375VM	Praxair	Cr_3C_2-25wt.%NiCr	21.34	33.25	51.71	Narrow	6.6955	93.4
PSU blend No. 9	Novamet/AEE	Cr_3C_2-18wt.%Ni	8.71	51.87	91.26	Broad	7.2737	>99.0

vestigation. Several "off-the-shelf" powders were purchased and investigated for use in applying wear-resistant coatings. These powders were met with mixed success, which led to preparation of various powder blend formulations to improve the wear-resistant properties of the cold spray coatings. Table 4 lists the various powders, powder size distributions, density, and mean particle diameter used in applying the different coatings. More than five different Cr_3C_2-25wt.%NiCr powders were purchased with different particle size distributions and average particle diameters. With the exception of TAFA 1375V, most of the "off-the-shelf" powders did not build up well. To better understand the poor coating buildup, the powders were investigated for density, size distribution, morphology, and average diameter. In addition, to achieve a wear-resistant coating for future developmental efforts with and without solid self-lubricating capabilities, several formulations were sprayed using Novamet pure nickel powder (Novamet Specialty Products Corp., Wyckoff, NJ) and chromium carbide from AEE (AEE, Atlantic Equipment Engineers, Bergenfield, NJ). Table 3 briefly lists the major powder characteristics.

One of the biggest disadvantages to date regarding the cold spray technology is the lack of understanding and characterization of the feedstock (i.e., powders). Several companies have invested heavily into the processing and characterization of select powders for HVOF, HVAF, and other plasma spray technologies. As a result, significant improvements have been made in coating quality and property performance. As the cold spray process matures, the authors believe that powder vendors will soon develop specialty powders with specific powder characteristics that aid in improving the sticking coefficient and efficiency of the CS process, as well as the coating performance. Therefore, the authors believe a more detailed investigation of the powders is warranted in an effort to help explain the differences in coating buildup and performance.

3.2.1 Nickel Powder (C1). Figure 5 shows scanning electron micrographs of the morphology of select powders used for the various coatings applied in this investigation. As shown in Fig. 5(a) and (b), the nickel powder (Novamet) prepared by thermal decomposition is categorized as being slightly porous. The measured density (8.4886 g/cm^3) of the nickel powder was determined to be 95.6% of its theoretical density and performed well with the CS process. The Novamet nickel powder used resulted in nickel coatings that were easy to build up with high coating densities. The high particle velocity of the impinging powders on the substrate surface results in the porosity within the nickel powder collapsing due to the plastic deformation, forming a very dense coating. The nickel powder was characterized as having a broad particle size distribution (Fig. 6) with a mean particle diameter [$D(v\ 0.5)$] of 15.72 μm as measured by laser light scattering technique.

3.2.2 PSU Blend No. 1 and No. 2: Cr_3C_2-25Ni (C2-C3). Figures 5(c) and (d) show the morphology of PSU blend No. 1: Cr_3C_2-25wt.%Ni. The powder blend is a mixture of nickel (Novamet) and Cr_3C_2 (Cerac, Inc.) powder. The Cr_3C_2 powder is characterized as being very dense, with a sharp faceted morphology. The high density of the Cerac Cr_3C_2 powder is believed to be one of the limiting factors with attempts at increasing the average Vickers hardness number of this powder blend. The Cr_3C_2 (Cerac) powders were too dense, resulting in poor incorporation within the CS coating. The high density of the Cr_3C_2 powders resulted in the powders being deflected (bouncing off) from the surface rather than incorporated into the cold sprayed coating. Although this resulted in coating densification, a limited volume fraction of Cr_3C_2 was being incorporated into the coating, resulting in the lower than expected hardness. PSU blend No. 2 (C3) differed from PSU blend No. 1 (C2) in that it had a larger particle size (−200/+325) distribution with the same high particle density.

3.2.3 PSU Blend No. 3: Cr_3C_2-15wt.Ni (C5) and No. 9: Cr_3C_2-18wt.Ni (C4). The powder morphology of PSU blend No. 3 Cr_3C_2 (AEE)-25wt.%Ni (Novamet) is shown in Fig. 5(e) and (f). The Cr_3C_2 powder from AEE is characterized as being slightly more porous than the Cr_3C_2 from Cerac, Inc. with a broad particle size distribution and $D(v, 0.5)$ of 65.35 μm. The

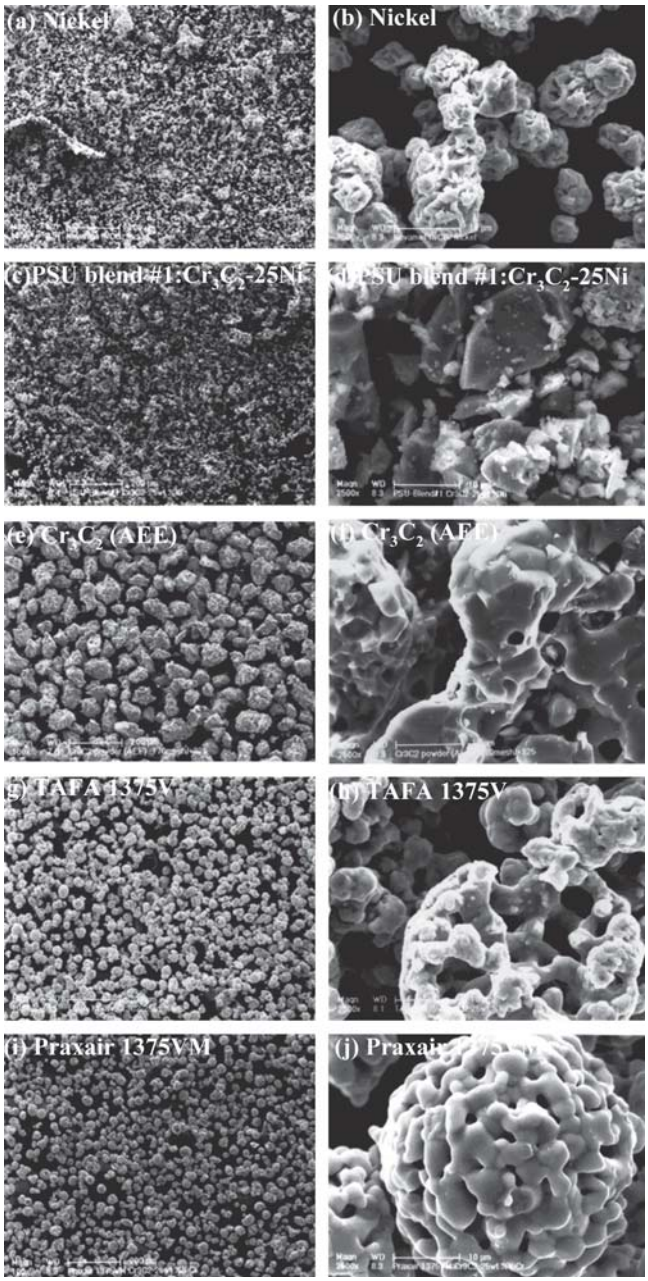

Fig. 5 Scanning electron micrographs showing the morphology of (a) and (b) nickel, (c) and (d) PSU blend No. 1: Cr_3C_2 (Cerac)-25wt.%Ni, (e) and (f) Cr_3C_2 (AEE) powder used in blends C4 and C5, (g) and (h) TAFA 1375V: Cr_3C_2-25wt.%NiCr, and (i) and (j) Praxair 1375VM: Cr_3C_2-25wt.%NiCr powders used in applying cold spray coatings on 4140 alloy

AEE Cr_3C_2 was determined to be 5.5496 g/cm^3, which is approximately 82% of the theoretical density for Cr_3C_2. The lower particle density combined with larger particle size resulted in increased volume concentrations of Cr_3C_2 particles incorporated into the various cold spray coating blends and thus slightly higher HV values. The smaller nickel powder size combined with larger open pores within the AEE Cr_3C_2 powder allowed the nickel powder to become incorporated (penetrate) within the open structure of the Cr_3C_2 where they plastically deformed, resulting in increased Cr_3C_2 sticking coefficients and thus increased Cr_3C_2 volume fractions and HV values. In addition, on impact, the porous Cr_3C_2 powder absorbed the impact energy by densifying and fracturing, reducing the number of Cr_3C_2 particles "bouncing off" the surface of the substrate. However, because the powders were blends and not chemically reacted, there was still a maximum Cr_3C_2 volume incorporation into the coating that could be obtained regardless of the binder concentration. The maximum Cr_3C_2 volume fraction was obtained with 15 wt.% Ni binder (C5). This is primarily the result of the hard chromium carbide powders not being completely surrounded by the soft metallic binder phase (nickel) as is often observed with agglomerated and sintered powders.

3.2.4 TAFA 1375V: Cr_3C_2-25NiCr (C6). The highest average Vickers hardness numbers were obtained for the TAFA 1375V powder and is primarily the result of the powder characteristics. The particle size distribution (Fig. 6 and Table 4) is characterized as being slightly broader than the other "off-the-shelf" powders with a $D(v, 0.5)$ of 35.36 μm. The measured density of the TAFA 1375V was determined to be 7.2947 g/cm^3, which is greater than 99% of the theoretical value of Cr_3C_2-25wt.%NiCr. The morphology of the TAFA 1375 agglomerated and sintered powder is shown in Fig. 5(g) and (h). The powders are characterized as being somewhat porous. The observed porosity is not in agreement with the measured density of the powders. Upon further investigation, it was determined that the TAFA 1375V powder was slightly rich in the metallic phase (i.e., NiCr). As a result of this increased softer binder phase, coating consolidation and buildup occurred with the CS process. The combination of the porosity and increased binder phase of the agglomerated and sintered powder resulted in particle deformation and particle consolidation, allowing the coating thickness to build up readily.

3.2.5 Praxair 1375VM: Cr_3C_2-25NiCr (C7). Finally, because of the success of the TAFA 1375V powder, additional powder was specially purchased to try and reproduce the TAFA 1375V powder performance. Praxair 1375VM was produced closer to the TAFA 1375V design specification with a fairly narrow particle size distribution (Fig. 6) and a $D(v, 0.5)$ of 33.25 μm. The powder density was 6.6955 g/cm^3, which is approximately 93.4% of the theoretical density value. The agglomerated and sintered powder morphology of Fig. 5(i) and (j) again shows that the powder is fairly porous and was very similar to that of the TAFA 1375V (Fig. 5g and h). However, although this powder was processed to the specification of the TAFA 1375V powder, it did not perform as well as the TAFA 1375V. The results suggested that the Praxair 1375VM powder was closer to the stoichiometric values and not rich in the metallic (NiCr) binder phase (as compared with the TAFA 1375V powder).

Based on the analyzed powder characteristics, a Cr_3C_2-based CS feedstock of agglomerated and sintered powders would have a uniform composition (preferably rich in NiCr) and microstructure (open porosity) to allow coating buildup and uniform average Vickers hardness number values. Based on the powder characterization, it is believed that a slightly higher concentration of the NiCr (approximately 27%) would perform very well with the cold spray process. As previously discussed (Fig. 3a and b), powder blend coatings allow wide average HV distributions and greater tailorability, and thus

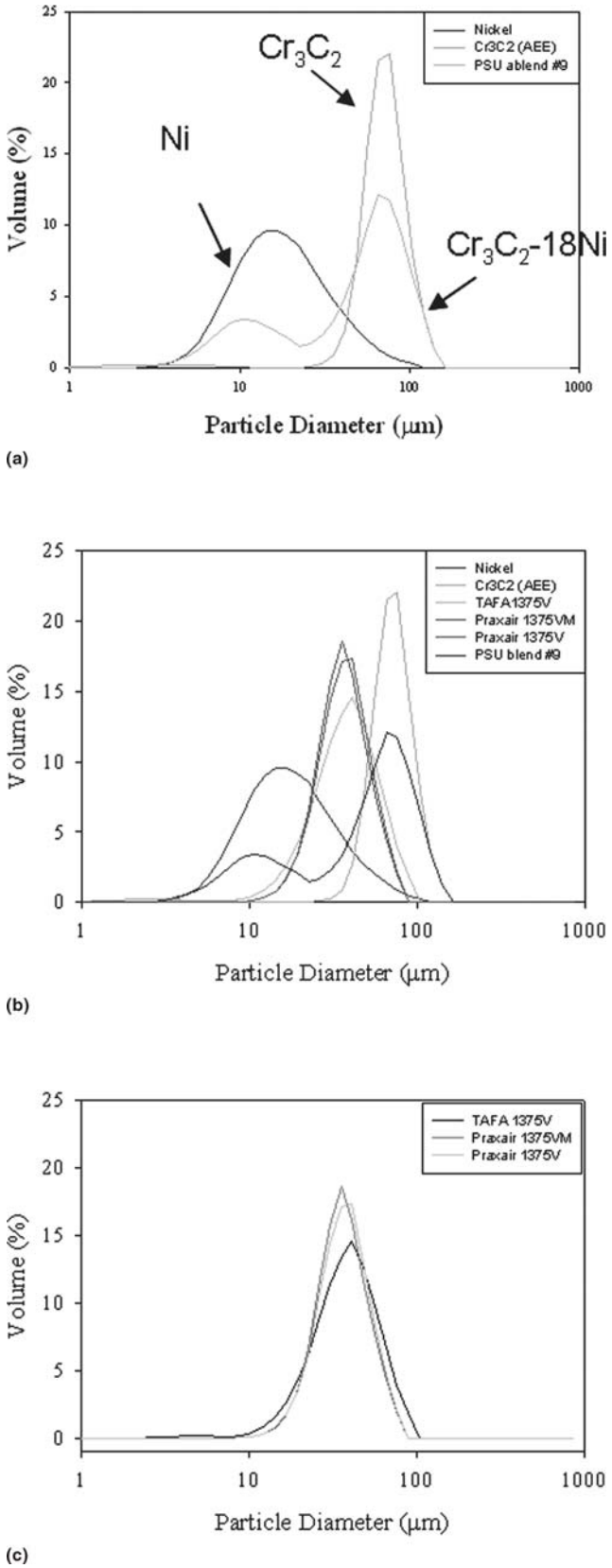

Fig. 6 Particle size distributions. (a) Nickel, Cr_3C_2 (AEE), and Cr_3C_2 (AEE)-18wt.%Ni (PSU blend No. 9). (b) Powders used for blends. (c) TAFA 1375V, Praxair 1375V, and Praxair 1375VM powders

wear resistance, especially when mating component wear is a concern.

3.3 X-ray Diffraction

XRD was performed to determine/confirm whether the chromium carbide concentration was altered from the original starting blend composition as compared with the coating material (to help explain the variations in coating hardness) and to determine whether crystallographic phase changes occurred during the cold spray process. In general, little change in the coating composition is observed for cold spray coatings as oxidation and phase transformation that occur due to increased particle or substrate temperatures are not inherent to the cold spray process. However, when mixing powder blends with hard, wear-resistant particles (carbides, nitrides, oxides), solid lubricants (sulfides), and soft metallic powders, variation in the coating composition can be observed that is caused by the hard carbide particles not undergoing plastic deformation and bonding to the substrate or previous coated layer. To show and confirm this, select XRD patterns were performed and compared with the Joint Committee for Powder Diffraction Standards (JCPDS), now known as the International Center for Diffraction Data (ICDD).

Figure 7(a) shows the XRD pattern of the pure nickel powder, chromium carbide powder, and Cr_3C_2-25wt.%Ni blend feedstocks prior to applying the cold spray coatings. As observed in Fig. 7(a), all of the powders were polycrystalline, with nickel powder being of the cubic crystallographic phase (JCPDS-ICDD No. 4-850) (Ref 17), and the chromium carbide powder being primarily of the orthorhombic crystallographic phase (Cr_3C_2, JCPDS-ICDD No. 35-804) (Ref 17) with a small volume fraction of the hexagonal (Cr_7C_3, JCPDS-ICDD No. 11-550) (Ref 17) crystallographic phase being detected. Due to the complexity of the diffraction patterns and the various overlaps of the planes of diffraction for the various compositional phases, detection of pure chromium (cubic) or delta chromium nickel (cubic) was not confirmed. To quantify the various phase mixtures, the internal and external standard methods were used to determine the weight percent of chromium carbide in the powder blend comprising the feedstock for the various cold spray deposition conditions in which the composition of the powder was already known. The intensities of the various crystal structures (i.e., phases) within the coating were then compared with that of the starting raw material with any deviations being attributed to a decrease in chromium carbide weight fraction.

Good agreement was observed between the volume intensities of each of the phases and the known starting composition. For example, for the Cr_3C_2-25wt.%Ni, the weight fraction of Cr_3C_2 was found to be 72.8%, which is very close to the 75.0% theoretical value. The small differences were attributed to nonuniform powder mixtures, differences in x-ray absorption coefficients, and variation in the Cr_7C_3 phase content from the raw feedstock. To determine the relative amount of chromium carbide and nickel within the cold spray coating, the volume intensities were determined after various background corrections, Kα2 stripping and peak smoothing using Philips (Eindhoven, The Netherlands) analytical software was performed. The volume intensities of the cold spray coatings were then compared

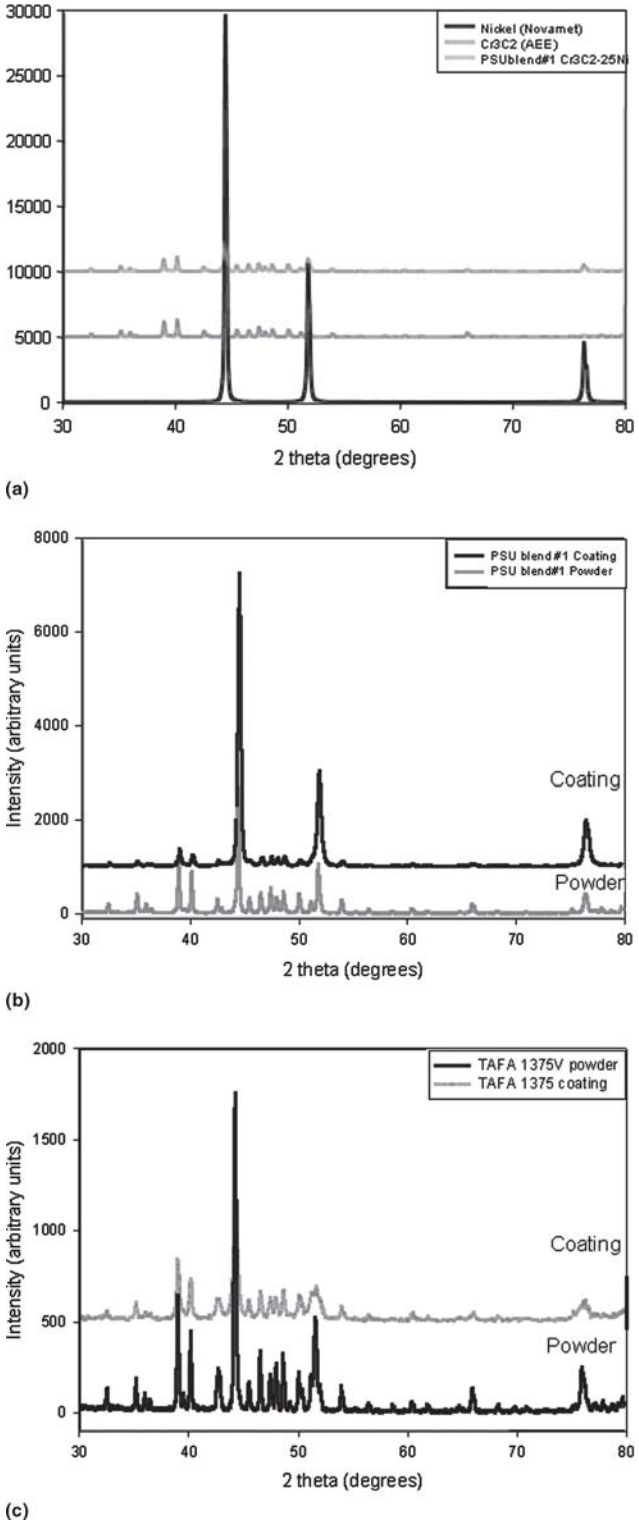

Fig. 7 X-ray diffraction patterns. (a) Nickel, chromium carbide, and PSU blend No. 1 powders. (b) PSU blend No. 1 powder and cold spray coating. (c) TAFA 1375V powder and CS coating. The coatings were all applied on 4140 alloy steel.

with the volume intensities of the corresponding known powder blend or raw powder stock material using the following equation to determine the chromium carbide weight fraction:

$$X_{Cr_3C_2} = (I\{111\}_{Ni}/(I\{121\}_{Cr_3C_2})(I\{111\}_{Ni}/(I\{111\}_{Ni} + I\{121\}_{Cr_3C_2}))$$

where $X_{Cr_3C_2}$ is the weight fraction of chromium carbide, $I\{121\}_{Cr_3C_2}$ is the volume intensity of the set of (121) chromium carbide diffraction planes, and $I\{111\}_{Ni}$ is the volume intensity of the (111) set of nickel diffraction planes. With the exception of the agglomerated and sintered powders, all of the blends showed a reduction in chromium carbide content (discussed below) that was confirmed by the optical and scanning electron microscopy analysis in the next section.

When comparing the diffraction patterns of the feedstock to the cold spray coatings, several differences were observed (Fig. 7b). In the case of the various coatings using the powder blends, a reduction in the relative intensity of the chromium carbide peak was always observed for the blends containing 15 to 25 wt.% Ni. This confirmed that chromium carbide was not being incorporated into the cold spray blend coating most likely due to chromium carbide not plastically deforming, but rather "bouncing off" the substrate surface. In addition to the lower-than-expected chromium carbide intensity, the diffraction peak for the nickel (cubic) phase was more broad and often shifted, which is indicative of an increase in nonuniform strains within the nickel matrix caused by plastic deformation. As a result of these strains, determination of the various phases present within the coating was subject to some error, and therefore the volume concentration of the various phases were reconfirmed using analytical software in combination with optical and scanning electron microscopy of polished coating cross sections. In addition, the peak positions for the nickel phase appear to be shifted from the original powder pattern and strongly suggest residual stresses present in the coating. In general, based on the direction of the peak shifting, the residual stresses were compressive in nature, which is supported by the physics of the cold spray process, resulting in compressive stresses within the coating due to the nature of particles impinging on the substrate surface acting to densify it. In general, the powder blends always showed a lower chromium carbide concentration due to the chromium carbide powders not being surrounded by a soft ductile matrix, which would allow it to bond to other particles.

In contrast, the TAFA 1375V powder and CS coating show almost the same identical diffraction pattern with respect to the relative intensities of the chromium carbide phase and delta-nickel chromium (Fig. 7c). However, it is again observed that nonuniform strains are observed in the NiCr phase as peak broadening was observed. In addition, the crystallinity of the NiCr phase is decreased due to the various degrees of strain induced into the particles resulting from plastic deformation in order for them to adhere to the 4140 alloy, as represented by the peak broadening. However, since the chromium carbide powders of the agglomerated and sintered TAFA 1375V are essentially surrounded by the soft metal matrix (NiCr), coating buildup occurred with little loss of chromium carbide phase observed and was confirmed by the optical and scanning electron microscopy investigation discussed in Section 3.4.

However, it should be noted that the hardness (Fig. 3b) of the coating can be tailored over a wide range of values up to the highest volume concentration of chromium carbide. This could allow a wide range of niche areas for the cold spray process. In

addition, it is believed that the volume concentration of the chromium carbide phase could be further increased if the chromium carbide powders were coated with a thin plastically deforming coating that would allow coating buildup. Increasing the volume concentration of the chromium carbide phase in the cold spray coatings would also allow further increases in hardness and increase the range of tailored average Vickers hardness numbers. It is clear that there is substantial potential for the cold spray process for niche areas in tailoring the surface hardness of temperature-sensitive materials that could not be applied by some of the other thermal spray techniques. The authors are in no way suggesting that cold spray will replace other thermal spray processes, but it does allow the flexibility in tailoring the wear-resistance properties of the material over a wider range of values. Again, one of the overall objectives of future work is to include solid lubricants into the wear-resistant surface for high-temperature applications where liquid lubricants cannot be used.

3.4 Scanning Electron Microscopy

Select samples were evaluated by OM and SEM to determine any microstructural differences that were attributing to the variations in the average Vickers hardness number. As shown in Fig. 8(a), the amount of chromium carbide (Cerac) incorporated into the CS coating is much less than the PSU blend No. 1 (Cerac Cr_3C_2 powder) preblended feedstock powder composition. Figure 8(b) shows a slightly higher volume concentration of chromium carbide incorporated into the CS coating (PSU blend No. 2). The differences in the amount of chromium carbide incorporation in the CS coatings were discussed in Section 3.2 (powder characteristics) and are attributed to the different particle size distributions. For comparison, the CS coating using TAFA 1375 powder (Fig. 8c) shows a much larger volume fraction of chromium carbide being incorporated into the coating. As a result, the average Vickers hardness numbers were greater for TAFA 1375V as compared with the various blended compositions. However, closer observations show that the blended compositions have a higher density than the TAFA 1375V, but the hardness values were lower. Therefore, if increased concentrations of Cr_3C_2 particles could be incorporated into the CS coating, higher HV values would be expected. These results support the XRD results suggesting lower carbide concentrations in the CS coatings.

3.5 Tribology

After the processing parameters were refined, several CS coatings were applied to 4140 alloy 24.4 × 25.4 × 6.35 mm (1 × 1 × ¼ in.) and, in addition to the uncoated substrate, were evaluated for wear resistance and friction coefficient determination. The coated and uncoated 4140 alloys were evaluated against 100Cr6 steel (mating material) for the tribology testing under dry conditions. The tribology parameters selected for the evaluation are shown in Table 5 using a CSEM THT tribometer S/N 4-116 instrument (Micro Photonics, Allentown, PA).

Two tribology tests were performed for each of the coating materials (Fig. 9). The average weight loss of the coating, mating material, and friction coefficient of the various CS coatings is listed in Table 6 and 7. The average friction coefficient for the uncoated alloy against 100Cr6 mating material was 0.725 ±

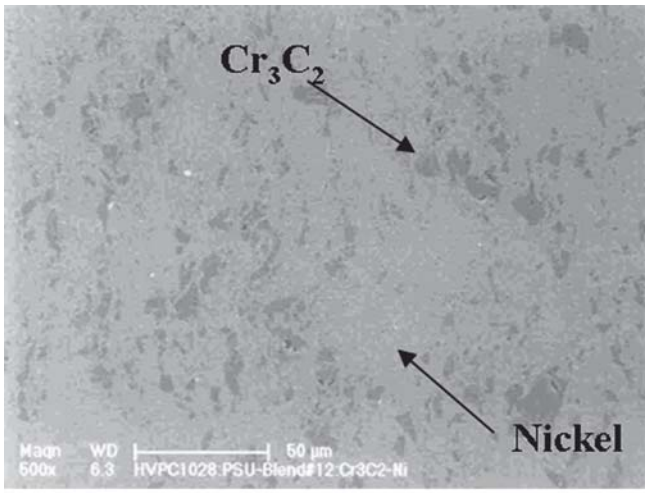

(a)

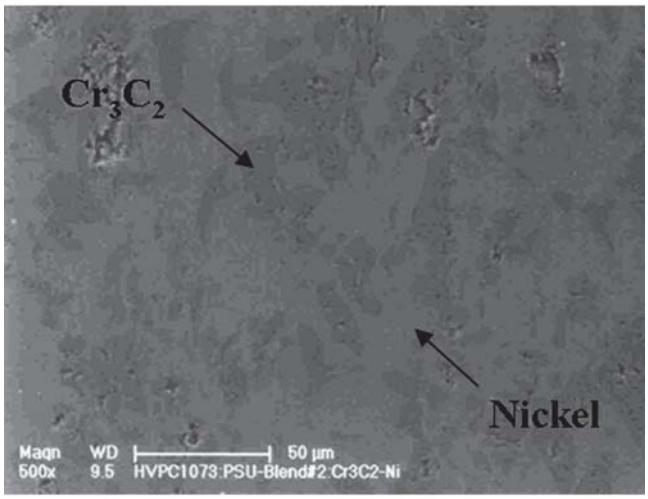

(b)

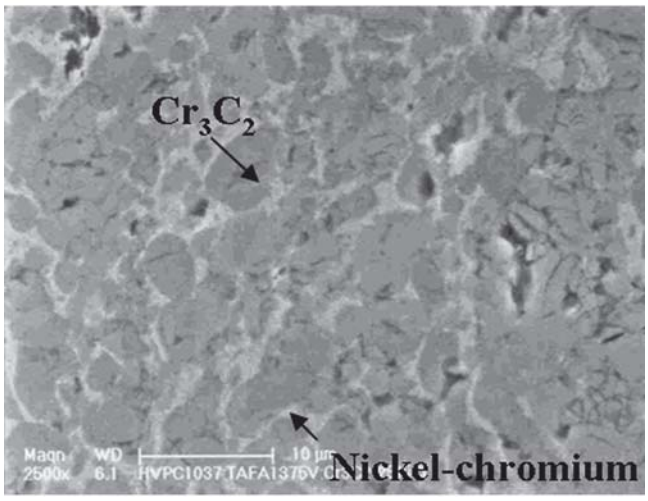

(c)

Fig. 8 Scanning electron micrographs of polished cross sections of CS coatings. (a) PSU blend No. 1, Cr_3C_2-25wt.%Ni. (b) PSU blend No. 2, Cr_3C_2-25wt.%Ni. (c) TAFA 1375V, Cr_3C_2-25wt.%Ni. The coatings were all applied on 4140 alloy steel.

Table 5 Major experimental parameters for tribology experiments

Parameter	Value
Load, N	5.00
Distance, E^{-3} km	540.0
Speed, cm/s	5.00
Radius, mm	3.00
Test time, h	3
Atmosphere	Air
Humidity	~26% (but varied between 24-32%)
Temperature	Ambient (~22-23 °C)
Lubrication	No
Mating material	6 mm diam 100Cr6 (low-carbon steel)

0.017. In comparison, the friction of the nickel, TAFA 1375V, and PSU blend No. 2 HVPC coatings was 0.824, 0.891, and 0.786, respectively. The average mean friction coefficient of the various coatings evaluated under dry conditions suggests that the PSU blend coating has the lowest mean friction values. However, in general, the friction increased with increasing time for all coatings tested under dry conditions, as shown by the friction profiles (Fig. 9). Preliminary trials were performed with 5 and 10 N loads and evaluated for wear and friction coefficient determination. Based on the data in Table 6 and 7, the wear rate of the 4140 alloy steel was fairly uniform with linear wear rates. The volume of material was estimated from a CMC six-axis machine that measured the wear profiles. A minimum of four measurements taken 90° apart were made to obtain a statistically weighted average loss of the samples. The wear profile (Fig. 10) as measured by the CMC machine appeared to be fairly uniform for the 4140 alloy (smooth surface). However, most of the CS Cr_3C_2-based coated samples did not have a smooth uniform surface finish, and it was very difficult to accurately determine the amount of wear for the coating. As a result, the degree of wear from the tribology test was based on the weight loss of the coating using a high precision balance. The results of the select samples are shown in Table 6 and 7. Overall, the chromium carbide coatings showed significant improvements in the wear rates as compared with the uncoated 4140 alloy, but additional testing is required to better understand the wear rates and friction coefficients. In addition, measurements and calculations were performed on the mating material (100Cr6 6 mm diam ball) to determine the wear of the mating material against the various coatings. However, due to the nonuniform wear patterns of the 6 mm diam 100Cr6 ball, this was more challenging as shown by the optical micrographs in Fig. 11.

The nonuniform wear patterns of the mating material (100Cr6) are believed to be associated with the varying degrees of surface finish. It should be noted that prior to the start of the tribology tests, the coated surfaces were ground to a specific surface finish for the coatings. However, due to the varying microstructures and degree of porosity, deviations in the surface roughness/finish occurred that may have influenced the wear patterns and the friction coefficients.

Additional sets of trial experiments were performed with a higher load of 10 N and under sand-oil lubricated condition. The type of lubrication used was DTE hydraulic oil with 20 wt.% Iraq sand (more aggressive environment). The tribology results appeared to show mixed results as to which coating performed the best under lubricated conditions. It appeared that some of the coatings gained weight due to the lubricant being incorporated into the porous coatings. These results are not discussed. The differences in the wear results from the 5 and 10 N loads are believed to be the result from localized changes in friction and coating microstructure. However, depending on the wear application it is not adequate to only look at the amount of wear associated with the coating material. Often it is important to consider both the coating and the mating material wear rates. For this effort, the PSU blend No. 2 coating showed similar wear results for both the Cr_3C_2-based coating and the 100Cr6 mating material. Similarly, the TAFA 1375V CS coating showed the least amount of wear, but increased amount of weight loss for the mating material. Therefore, it is important to consider the results of each test and consider the results based on the desired application. For the purpose of this study, the authors were looking for a coating material that had uniform wear against 100Cr6 hardened alloy steel (1000 $HV_{0.300}$).

3.6 Bond Strength

Using an Instron IX Automated Materials Testing System (Instron Corp., Norwood, MA), CS TAFA 1375V and PSU blend No. 2 coatings were evaluated for bond strength according to ASTM standard C 633-01. Special 25.4 mm diam specimens were prepared for applying both TAFA 1375V and PSU blend No. 2 CS coatings. The coated specimens were bonded to a mating surface using a Loctite Hysol E-214HP adhesive bonding agent (Henkel Corp.-Industrial, Rocky Hill, CT). Increasing tensile load was applied with a constant cross head rate of 0.013 mm/s (0.030 in./min) until rupture occurred. The average bond strength of the TAFA 1375V and PSU blend No. 2 samples was 27.5 ± 3.5 MPa (3.99 ± 0.716 ksi) and 39.5 ± 2.5 MPa (5.727 ± 0.525 ksi), respectively. The adhesive bond strength of the Cr_3C_2-based coatings applied by the cold spray process in this investigation is comparable to the low to mid range of those values reported in the literature for thermal sprayed Cr_3C_2-NiCr coatings (30 to 70 MPa) (Ref 18-21). The method of coating deposition, the surface condition, surface roughness, and so forth, all have considerable impact on the degree of coating adhesion. In general, the coatings failed primarily due to adhesive failure and not cohesive failure. Further testing and evaluation are planned for the remaining coating materials.

3.7 Potential Hybrid Process Combining Cold Spray and Laser Processing

Microscopy of the polished cross sections in combination with low hardness measurements of some of the Cr_3C_2-25wt.%NiCr (TAFA 1375V) coatings strongly suggested that the cold spray coatings contained macroporosity and microporosity (Fig. 8). This porosity is believed to be the main factor in the relative low average Vickers hardness numbers of the various chromium carbide based cold spray coatings ranging from 300 to ~575 $HV_{0.500}$, depending on the deposition parameters. In an effort to increase the HV, laser glazing trials using a 3 kW YAG laser were performed. Several trials were performed to determine whether laser glazing would further improve the coating quality, density, and microstructure, and thus the cold spray coating properties (particularly HV). The two primary laser parameters investigated were laser power and traverse speed. Figure 12(a) shows a digital image of several laser passes over the

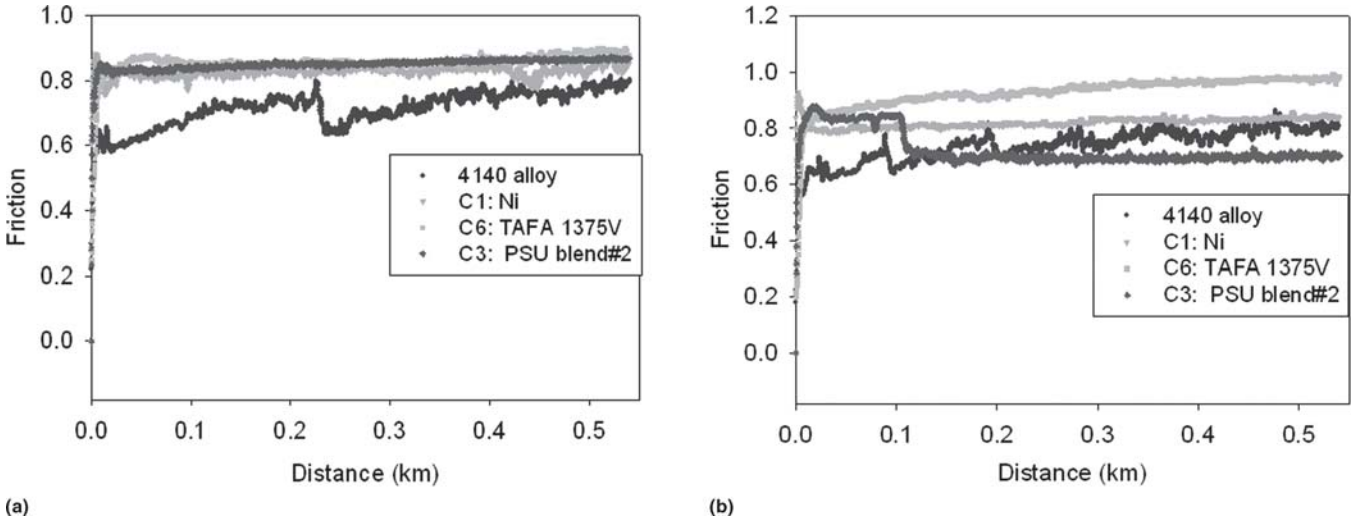

Fig. 9 Friction profiles for 4140 alloy, C1, C3, and C6 CS coatings tested against 100Cr6 mating surface with (a) 5 N and (b) 10 N loads

Table 6 Tribology results for CS coatings tested under the following conditions: 5 N, no lubricant, R = 3 mm, 79.6 rpm, and 0.54 km distance traveled

Coating	$HV_{0.300}$	Average coating loss, g	Average mating material loss, g	Average friction coefficient
Uncoated 4140 alloy	444 ± 25	−0.00178	−0.00031	0.725
Nickel coating	310 ± 52	−0.00447	−0.00011	0.824
PSU blend 2: Cr_3C_2-25wt.%Ni	**449 ± 28**	**−0.00045**	**−0.00007**	**0.786**
TAFA 1375V: Cr_3C_2-25wt.%NiCr	775 ± 127	−0.00242	−0.00093	0.891

Table 7 Tribology results for CS coatings tested under the following conditions: 10 N, no lubricant, R = 3 mm, 159.2 rpm, and 0.54 km distance traveled

Coating	$HV_{0.300}$	Average coating loss, g	Average mating material loss, g	Average friction coefficient
Uncoated 4140 alloy	444 ± 25	−0.00337	−0.00007	0.517
Nickel coating	310 ± 52	−0.01997	−0.00034	0.702
PSU blend 2: Cr_3C_2-25wt.%Ni	449 ± 28	−0.00483	−0.00061	0.752
TAFA 1375V: Cr_3C_2-25wt.%NiCr	**775 ± 127**	**−0.00220**	**−0.00179**	**0.708**
PSU blend 3: Cr_3C_2-15wt.%Ni	*483 ± 58*	*−0.00030*	*−0.00108*	*0.663*
PSU blend 9: Cr_3C_2-18wt.%Ni	*432 ± 98*	*−0.00033*	*−0.00121*	*0.664*

surface of a cold sprayed Cr_3C_2-25wt.%NiCr coating. Preliminary trials showed densification of the surface material with pore coalescence near the bottom of the laser glaze melt pool. In general, the melt pool depth of penetration can be controlled by adjusting the laser power, beam size and traverse speed. Also observed in Fig. 12(b) is cracking near the interface associate with pore coalescence and shrinking of the coating. Although no

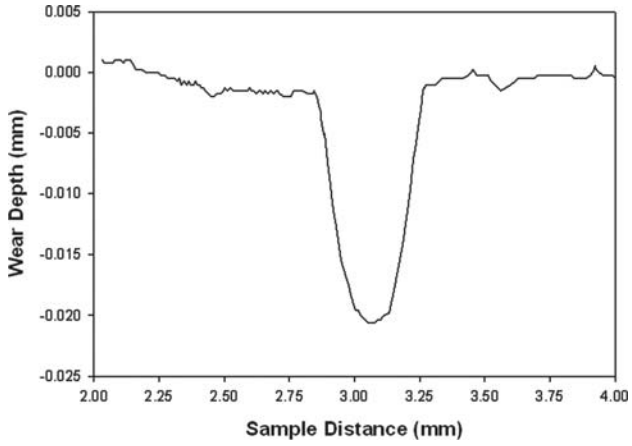

Fig. 10 Wear depth as a function of wear track width

cracking was observed in the glazed region, some cracking along the sides was observed. Backscattered scanning electron micrographs are shown in Fig. 12(c) and (d) and show a very dense microstructure. However, due to the high temperatures associated with the laser glazing and localized surface melting, some dissolution of the chromium carbide phase occurred resulting in a phase transition. However, similar phase transitions also occur for other techniques. The preliminary results show a significant improvement in the coating hardness. The average Vickers hardness number before and after laser glazing was ~450 and 1015 $HV_{0.500}$, respectively, which is more than a 100% increase in the average Vickers hardness of the "as-sprayed" coating. The increase in hardness is attributed to the densification/solidification of the CS coating. However, additional efforts are required as pore coalescence occurred beneath the coating surface, which could act as failure initiation sites for delamination (Fig. 12b). Defocusing and scanning the laser beam over the surface of the coating should help to minimize the entrapped porosity resulting in a very dense coating with high hardness as shown in Fig. 13. Figure 13 shows the cross section of a PSU

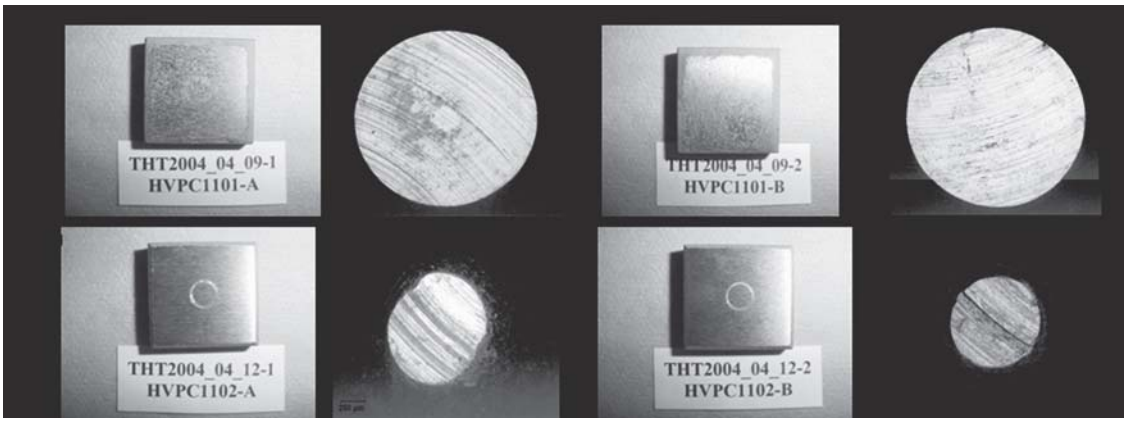

Fig. 11 Digital images of wear block and wear pattern of 6 mm diam mating material (100Cr6) for (a) TAFA 1375 and (b) PSU blend No. 2 coatings on 4140 alloy. Tested under the following conditions: 5 N, 3 mm radius, 5 cm/s, and no lubricant

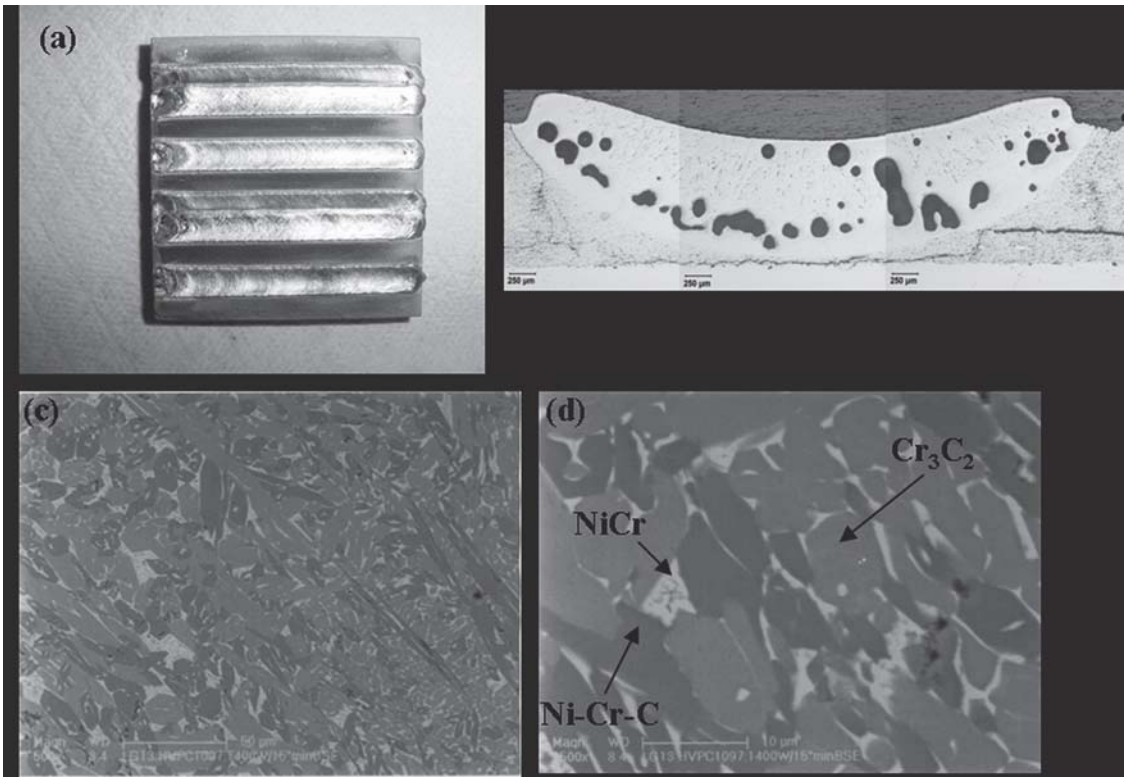

Fig. 12 (a) Digital images of surface. (b) Optical micrograph of polished cross section. (c) and (d) Backscattered electron micrographs of polished cross sections of a laser glazed cold sprayed TAFA 1375V: Cr_3C_2-25wt.%NiCr coating on 4140 alloy. Laser processing parameters: 3 kW YAG at 1900 W with traverse speed of 38.1 mm/min

blend No. 2 CS coating that was laser glazed, showing increased density and no apparent cracking in the glazed region. Therefore, adding a laser attachment to the cold spray process could result in a new hybrid coating technology addressing some of the limitations of the laser cladding process.

4. Conclusions

The cold spray (CS) process was successful in applying Cr_3C_2-25wt.%NiCr and Cr_3C_2-25wt.%Ni coatings on 4140 alloy for wear-resistant applications. Average Vickers hardness numbers of the Cr_3C_2-based coatings range from 300 to 900 $HV_{0.300}$, which strongly suggests that the hardness (and thus wear resistance) can be tailored over a wide range of values to meet a variety of hardness specifications. In general, optimized standoff distance, powder feed rate, traverse speed, and nozzle design led to more than a 57 and 37% increase in average Vickers hardness number for the agglomerated and sintered powder and powder blends, respectively. The bond strength of the cold spray specimens (24 to 44 MPa) were comparable to the lower

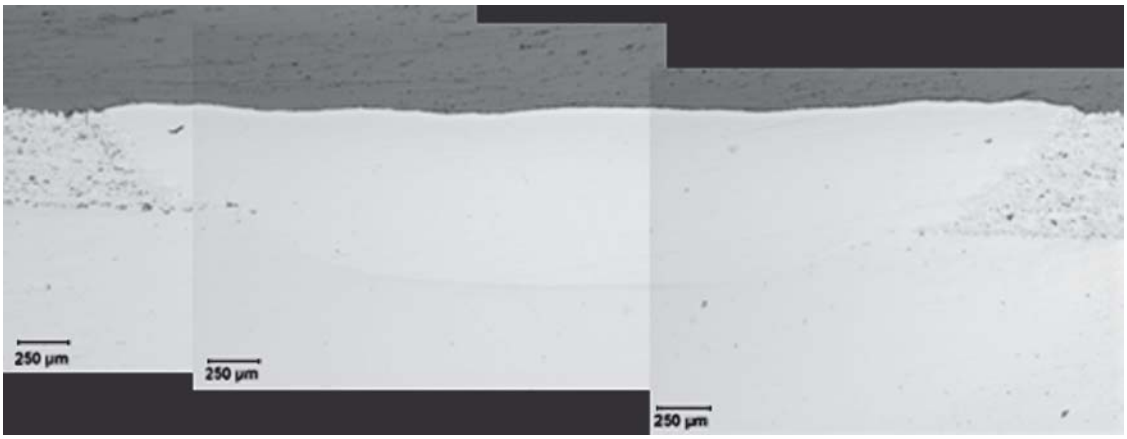

Fig. 13 Optical micrograph of laser glazed surface of PSU blend No. 2 Cr_3C_2-25wt.%Ni, showing little porosity due to the increased density of the cold spray coating and dissolution with the substrate due to the increased energy. Laser processing parameters: 3 kW YAG at 2300 W with traverse speed of 6.35 mm/s (381 mm/min)

end values (30 to 70 MPa) of HVOF sprayed Cr_3C_2-based coatings. Combining the cold spray process with laser glazing technique resulted in the highest $HV_{0.500}$ of approximately 1015 $HV_{0.500}$ and shows promise for refurbishing complex geometries. Tribology tests showed that the wear rates of Cr_3C_2-based coatings are significantly better than the 4140 alloy. The presented results strongly suggest that the cold spray process is a new, but versatile process that could be used to tailor the coating composition, friction coefficient, hardness, and wear resistance.

Acknowledgment

This research was sponsored by the United States Manufacturing Technology (ManTech) Program, Office of Naval Research, under Navy Contract N00024-02-D-6604. Any opinions, findings, conclusions, or recommendations expressed in this material are those of the authors and do not necessarily reflect the views of the U.S. NAVY.

References

1. A.P. Alknimov, V.F. Kosarev, and A.N. Papyrin, "Cold Gas Dynamic Spray Method for Applying a Coating," U.S. Patent 5,302,414 April 12, 1994
2. Cold Gas-Dynamic Spray Method, *FutureTech,* 1998, Aug, No. 224, p 1-15
3. M.F. Amateau and T. Eden, High Velocity Particle Consolidation Technology, *iMAST Quarterly,* 2000, No. 2, p 3-6
4. H.K. Kan and S.B. Kank, Tungsten/Copper Composite Deposits Produced by a Cold Spray, *Scr. Mater.,* 2003, **49,** p 1169-1174
5. H.Y. Lee, Y.H. Yu, Y.C. Lee, Y.P. Hong, and K.H. Ko, Interfacial Studies between Cold-Sprayed WO_3, Y_2O_3 Films and Si Substrate, *Appl. Surf. Sci.,* 2004, **227,** p 244-249
6. T.H. Van Steenkiste, J.R. Smith, and R.E. Teets, Aluminum Coatings via Kinetic Spray with Relatively Large Powder Particles, *Surf. Coat. Technol.,* 2002, May 15, **154**(2), p 237-252
7. T.H. Van Steenkiste, J.R. Smith, R.E. Teets, J.J. Moleski, D.W. Gorkiewicz, R.P. Tison, D.R. Marantz, K.A. Kowalsky, W.L. Riggs, P.H. Zajchowski, B. Pilsner, R.C. McCune, and K.J. Barnett, Kinetic Spray Coatings, *Surf. Coat. Technol.,* 1999, Jan 10, **111**(1), p 62-71
8. R.S. Lima, J. Karthikeyan, C.M. Kay, J. Lindemann, and C.C. Berndt, Microstructural Characteristics of Cold-Sprayed Nanostructured WC-Co Coatings, *Thin Solid Films,* 2002, **416,** p 129-135
9. R.C. McCune, A.N. Papyrin, J.N. Hall, W.L. Riggs, and P.H. Zajchowski, An Exploration of the Cold Gas-Dynamic Spray Method for Several Materials Systems, *Proc. Eighth National Thermal Spray Conference* (Houston, TX), C.C. Berndt and S. Sampath, Ed., ASM International, 1995, p 1-6
10. C.J. Li and W.Y. Li, Deposition Characteristics of Titanium Coating in Cold Spraying, *Surf. Coat. Technol.,* 2003, **167,** p 278-283
11. R.C. McCune, W.T. Donlon, E.L. Cartwright, A.N. Papyrin, E.F. Rybicki, and J.R. Shadley, Characterization of Copper and Steel Coatings Made by the Cold Gas-Dynamic Spray Method, *Proc. Ninth National Thermal Spray Conference* (Cincinnati, OH), C.C. Berndt, Ed., ASM International, 1996, p 397-403
12. H. Assadi, F. Gartner, T. Stoltenhoff, and H. Kreye, Bonding Mechanism in Cold Gas Spraying, *Acta Mater.,* 2003, **51**(15), p 4379-4394
13. M. Grujicic, J.R. Saylor, D.E. Beasley, W.S. DeRosset, and D. Helfritch, Computational Analysis of the Interfacial Bonding between Feed-Powder Particles and the Substrate in the Cold-Gas Dynamic-Spray Process, *Appl. Surf. Sci.,* 2003, **219,** p 211-227
14. M. Grujicic, C.L. Zhao, C. Tong, W.S. DeRosset, and D. Helfritch, Analysis of the Impact Velocity of Powder Particles in the Cold-Gas Dynamic-Spray Process, *Mater. Sci. Eng.,* 2004, **A368,** p 222-230
15. M. Grujicic, C. Tong, W.S. DeRosset, and D. Helfritch, Flow Analysis and Nozzle-Shape Optimization for the Cold-Gas Dynamic-Spray Process, *Proc. Inst Mech. Eng. B: J. Eng. Manuf.,* 2003, **217,** p 1603-1607
16. J. German, Industry Warms Up to Promises of Cold Spray, Sandia Lab News, 2001, **3**(8), p 1-3
17. International Centre for Diffraction Data, ICDD-JCPOS Data of Crystallographic data, 12 Campus Blvd., Newton Square, PA
18. C.J. Li, G.C. Ji, Y.Y. Wang, and K. Sonoya, Dominant Effect of Carbide Rebounding on the Carbon Loss During High Velocity Oxy-fuel Spraying of Cr_3C_2-NiCr, *Thin Solid Films,* 2002, **419,** p 137-143
19. M.H. Staia, T. Valente, C. Bartuli, D.B. Lewis, C.P. Constable, A. Roman, J. Lesage, D. Chicot, and G. Mesmacque, Part II: Tribological Performance of Cr_3C_2-25% NiCr Reactive Plasma Sprayed Coatings Deposited at Different Pressures, *Surf. Coat. Technol.,* 2001, **146-147,** p 563-570
20. T. Sahraoui, N.E. Fenineche, G. Montavon, and C. Coddet, Structure and Wear Behaviour of HVOF Sprayed Cr_3C_2-NiCr and WC-Co Coatings, *Mater. Des.,* 2003, Aug, **24**(5), p 309-313
21. J. Li and C. Ding, Improvement in the Properties of Plasma-Sprayed Chromium Carbide Coatings Using Nickel-Clad Powders, *Surf. Coat. Technol.,* 2000, Aug, **130**(1), p 15-19